http://dx.doi.org/10.1016/j.ijplas.2021.103076

Study of dislocation-twin boundary interaction mechanisms in plastic deformation of TWIP steel by discrete dislocation dynamics and dislocation density-based modelling

Xiangru Guo [a,b], Chaoyang Sun[b,*], Chunhui Wang[b], Jun Jiang[c], M.W. Fu[d,#]

[a] Tianjin Key Laboratory for Advanced Mechatronic System Design and Intelligent Control, School of Mechanical Engineering, Tianjin University of Technology, Tianjin 300384, China

[b] School of mechanical engineering, University of Science and Technology Beijing, Beijing, 100083, China

[c] Department of Mechanical Engineering, Imperial College London, Exhibition Road, London, SW7 2AZ, UK

[d] Department of Mechanical Engineering, The Hong Kong Polytechnic University, Hung Hom, Kowloon, Hong Kong

Abstract

Deformation twins contribute to the unique deformation behaviors and characteristics in the plastic deformation of TWIP steels since twin boundary (TB) blocks the movement of dislocations and absorbs them in deformation process. On the other hand, dislocations can traverse TB. However, there is still no consensus on how TB influences the plastic deformation of TWIP steel among prior researches. Therefore, exploring the interaction between dislocation and TB in deformation is critical to understand the effects of twins on the macro deformation behaviors and exploiting the strengthening potential of the alloys. In this study, a dislocation-TB interactions model for TWIP steel was proposed, developed and implemented in discrete dislocation dynamics (DDD) simulation, the complicated dislocation reactions at the TB were determined by the energy criterion, which serves as a feasible approach to represent the micro deformation characteristics under different tension directions with respect to the twin plane normal of TWIP steel micropillar. Furthermore, the effect of dislocation type and reaction characteristic at the TB in DDD are incorporated into the conventional dislocation density-based (DDB) model, and then the improved DDB model is

used to quantitatively describe the macro plastic behavior of TWIP steel micropillar. The DDD simulation results show that the dislocation-TB interactions are related to the dislocation type and the angular relationship between loading direction and twin plane normal. The TB has a significant strengthening effect if the loading direction is perpendicular to the twin plane (0º) due to the increase of the back stress induced by the activated 60º dislocation pileups. For other orientations (45º and 90º), however, the strain hardening becomes negligible. Meanwhile, the stress and dislocation density-strain curves under different directions with respect to the twin plane normal are predicted by the improved DDB model and have a good agreement with the DDD simulation and experimental results. The research thus advances the understanding of dislocation-TB interaction mechanisms in plastic deformation of TWIP steels.

Keywords: TWIP steel, Deformation twins, Dislocation-TB interaction, Dislocation density, Discrete dislocation dynamics.

The Corresponding authors:

*Chaoyang Sun, E-mail Address: suncy@ustb.edu.cn

#M.W. Fu, Email Address: mmmwfu@polyu.edu.hk

1. Introduction

Twinning-induced plasticity (TWIP) steels have high strength, excellent plasticity and toughness, which meet the high strength and ductility requirements of automobile steels (Gao et al., 2000). TWIP steels have face-centred cubic (FCC) crystal structure with low stacking fault energy (SFE). In such a crystal structure, the lattice dislocations are more likely to be dissociated into partial dislocations when they are impeded. Under the favourable loading conditions, the stacking fault width between the partial dislocations is increased to form twins, and the simultaneous formation of the coherent twin boundary and incoherent twin boundary (Idrissi et al., 2010; Liang et al., 2019; Shen et al., 2013;Wang et al., 2017). Thus, a large number of dislocations between the twin lamellae mainly interact with the coherent twin boundary (TB), resulting in the strain hardening and accommodating the plastic deformation of TWIP steels.

To reveal the influence of twinning mechanism on plastic deformation, texture formation, flow stress and strain hardening, extensive researches on the plastic behavior of TWIP steels were conducted by using macro and micro experimental characterization and numerical simulations (Bouaziz et al., 2011; Dancette et al., 2012; De Cooman et al., 2018; Guo et al., 2017; Gutierrez-Urrutia and Raabe, 2012; Idrissi et al., 2010; Li et al., 2013; Liang et al., 2017; Lu et al., 2020; Mahato et al., 2017; Shen et al., 2013; Steinmetz et al., 2013; Sun et al., 2016; Wei et al., 2014). Currently, it is generally believed that the contribution of deformation twins to plastic strain is very small due to the low saturation value of twin volume fraction, and the effect of twins on crystallographic texture development stems from the interaction between TBs and the conventional {111} ⟨110⟩-type slip (De Cooman et al., 2018; Li et al., 2013). The underlying dislocation-TB interaction, however, is not clear. Furthermore, the deformation twins' contribution to flow stress and strain hardening is still a controversial issue. Some researchers believe that TBs are similar to grain boundaries

(GBs). TBs can effectively block dislocation slip and reduce the mean free path (MFP) of dislocations, resulting in a large number of dislocation pileups and the dynamic Hall-Petch strengthening effect. To name a few, Bouaziz et al. (2011) found that the TBs block dislocation movement and result in the increase of back stress, which can be up to ~50% of the total flow stress in tension deformation of TWIP steel. Zhou et al. (2016) also revealed that the TBs contribute to more than 25% flow stress in tension deformation of TWIP nanotwinned steel. However, there is another understanding that TBs should not be considered as the conventional high angle GBs for pinning the dislocations. To exemplify a few, Idrissi et al. (2010) observed that the perfect dislocations are dissociated into partial dislocations coordinating the plastic deformation when they moved to the TBs. Choi et al. (2018) also showed the transmission of partial dislocations through the TBs in TWIP steel micropillar compression test, and they assumed that the TBs associated strengthening is primarily caused by reducing the dislocation MFP. Some researchers also suggested that the twins have a little influence on macro flow stress and strain hardening behavior. For example, Liang et al. (2016) and Luo and Huang (2018) demonstrated that the contribution of deformation twins to flow stress and strain hardening rate is limited. Instead, the forest hardening via dislocations entanglement, contributes to about 90% of flow stress increase and strain hardening after yielding. Fu et al. (2018) evidenced the key role of forest dislocation hardening of TWIP steels by in-situ TEM characterization, and the twin-twin intersections further constructed a channel for the easy glide of dislocations, where the dislocations cross slip from one twin plane to the other. So far, there is no a well-accepted understanding of the influence of deformation twins on macro plastic behavior. It is difficult to explain the relevant findings obtained by different macro and micro experiments, and there is also a lack of capable experimental technique for in-situ observation and tracing of the instantaneous dislocation-TB interactions.

From the theoretical aspect, the flow stress is proportional to the square root of dislocation density as described in Taylor hardening law, which specifies the relationship between flow stress, strain hardening and dislocation density evolution in the plastic deformation of metallic materials (Allain et al., 2004; Bouaziz et al., 2011; Zhang et al., 2013). In the dislocation density-based (DDB) model proposed by Allain et al. (2004), the dislocation MFP was a critical variable in describing the dislocation density evolution. In describing the MFP, the TBs could effectively block the dislocations on the slip planes inclined to the TBs, and this description method has been widely used by researchers (Bouaziz et al., 2011; Steinmetz et al., 2013; Liang et al., 2015). The DDB model suggests that the dislocation density and strain hardening was increased dramatically in a small strain with the decreasing dislocation MFP. However, the results of TEM characterization by Choi et al. (2018) and Fu et al. (2018) showed that the dislocations can traverse the TBs into the slip planes in the twinned region. This is similar to the dislocation cross slip process in which the TBs only change the dislocation slip planes and directions. Therefore, the above DDB model could not accurately describe the influence of deformation twins on dislocation density and hardening behavior without considering the dislocation reactions at the TBs in describing the dislocation MFP.

To clarify the dislocation-TB interaction mechanisms and accurately incorporate the TBs into the dislocation MFP evolution model. From micro scale aspect, MD simulations showed that the screw dislocation may either propagate into the adjacent twinned region by traversing the TB or cross slip onto the TB, and the 60° dislocation dissociates into different partial dislocations slipping into the twinned domain as well as along the TB, dislocation-TB interactions are affected by dislocation line length, applied stress, local curvature (Jin et al., 2006; Jin et al., 2008; Xu et al.; 2016). Furthermore, Wang et al. (2017) demonstrated the multiple roles of deformation twins as the dislocation barrier, storage and channel for cross

slip, the highly organized TBs were beneficial to accommodating the plastic deformation under specific loading conditions, which ultimately contribute to the high strength and ductility of TWIP steels. In addition, the angular relationship between the loading direction and twin plane normal has an important influence on the dislocation reaction at the TBs. As shown in nanotwinned materials, different loading directions activate different slip systems and form different dislocation-TB interactions, and this leads to the orientation effect of twin on the macro mechanical response (You et al., 2013; Mianroodi and Svendsen, 2020). In those MD simulations, however, uncommonly high kinetic energy with the strain rate of more than 10^7 s^{-1} is assumed and assigned to the dislocation due to the computational requirement. The dislocation reaction requiring a higher energy barrier may occur under the high strain rate loading, leading to the distortion of dislocation reactions at the TBs in MD simulation. The MD simulations provide reference for further research to determine the dislocation reactions at the TBs.

Discrete dislocation dynamics (DDD) is based on the deformation theory of dislocations to simulate dislocations as linear defects in the elastic continuum materials. With the intrinsic length parameters such as Burgers vector, dislocation type, dislocation line direction and other intrinsic characteristics of dislocations being incorporated into DDD simulation, the simulation can accurately describe the evolution process of the dislocation-dislocation reactions and capture the nature of various deformation mechanisms in micro plastic deformation (Cai et al., 2013; Cui et al., 2014; El-Awady, 2015; Fan et al., 2015; Huang et al., 2020; Khan et al., 2004; Lavenstein et al., 2019; Li et al., 2014; Liu et al., 2009; Srivastava et al., 2017; Zhang et al., 2021; Zheng et al., 2016; Zhu et al., 2014). Regarding the DDD modeling of the dislocation-TB interactions, Fan et al. (2015; 2016) introduced the twins into the DDD framework to analyze the strain hardening of a Mg alloy (Hexagonal closed-packed material) and revealed that TBs act as a strong obstacle to dislocation slip and contributes

significantly to the overall hardening response. In addition, Wei et al. (2019) established a DDD model for FCC Cu coupling the dislocation-TB interactions and revealed the orientation effects of twins in compression. However, the TWIP steels with a considerably lower SFE than that of Cu and different dislocation reactions at the TBs have not been studied and modelled. Establishing a DDD model to reveal dislocation-TB interactions and their influence on macro flow stress and strain hardening behavior of TWIP steels is crucial and needed.

In view of the above analysis, the influence of dislocation-TB interactions on the plastic deformation of TWIP steels has not yet been well explored and explained based on the macro and micro experimental characterization and numerical simulation. Therefore, it was very meaningful to reveal dislocation reaction characteristics at the TBs and determine the twin's contribution to the macro mechanical behavior in the deformation of TWIP steels with low SFE. Aiming at this purpose, this study proposed and developed a DDD model to investigate the dislocation-TB interactions in the plastic deformation of TWIP steels. The critical resolved shear stresses for dislocation reactions at the TB were calculated based on the energy criterion. The dislocation-TB interactions and their topological changes were introduced into the DDD framework, the influence of twins on macro mechanical responses was analyzed by observing the dislocation evolution process near the TB under different loading directions. Furthermore, the observed dislocation-TB interaction mechanisms in DDD were embedded into a DDB model to evaluate how twins affect the yield stress and strain hardening behavior in the TWIP steels. The simulation results under different TB orientations by the improved DDB model had a good agreement with the DDD simulation and experimental results. The result also explained that twins' contribution to yielding and strain hardening behaviors were limited in the plastic deformation of TWIP steels.

2. Discrete dislocation plasticity coupling dislocation-TB interactions

2.1. Discrete dislocation plasticity framework

In DDD simulation, the dislocation is discretized into several linear segments containing

a mixed characteristic of edge dislocation and screw dislocation. The dislocation nodes connect each dislocation segment, the dislocation segments and nodes can occupy any slip plane position. The total force acting on the dislocation segment is given by:

$$f = f^{\mathrm{PK}} + f^{\mathrm{self}} + f^{\mathrm{image}} \tag{1}$$

where f^{PK} is the Peach-Koehler force, f^{self} is line tension, f^{image} is image force caused by the free surfaces, which can be calculated from Liu et al. (2009). The Peach-Koehler force calculation formula is as follows,

$$\mathbf{f}^{\mathrm{PK}} = \left(\boldsymbol{\sigma}\cdot\mathbf{b}\right)\times\boldsymbol{\xi} \tag{2}$$

where $\boldsymbol{\sigma}$ is the total of applied stress and stress field of the other dislocation segments, $\mathbf{b}$ is the Burgers vector of the dislocation segment, $\boldsymbol{\xi}$ is dislocation line direction.

The motion equation is then used to describe each segment of dislocation line. Implementation of a Peierls stress involves modification of the dislocation mobility law by treating the Peierls stress as internal friction in the standard manner (Olarnrithinun et al., 2013). As a simple model for dislocation motion in the over-damped regime, the velocity of each dislocation segment per unit length is determined by the total force acting on it divided by the viscous drag coefficient (Olarnrithinun et al., 2013),

$$v = \begin{cases} \dfrac{\left(f - \tau^{\mathrm{p}} b \cdot sign(f)\right)}{B} & \text{if } \left|f\right| > \tau^{\mathrm{p}} b \\ 0 & \text{else} \end{cases} \tag{3}$$

where v is the velocity of dislocation segment, τ^{p} is the Peierls stress. The viscous drag coefficient B is 10^4 Pa s for lattice dislocations in grains and 5×10^4 Pa s for twinning dislocations (the Shockley partial dislocation on TBs) (Wei et al., 2019).

2.2. Dislocation-TB interactions model for TWIP steel

In DDD simulations, a TWIP steel cubic cell with the grain size of l_g is employed to model a representative grain to avoid the influence of the GBs in polycrystalline, it is also easier to deal with the image force. The three dimensional rectangular Cartesian coordinate system is established, and the twin plane normal is selected as the Z axis. Here, the ABC plane is assumed the TB in the Thompson tetrahedron as shown in Fig.1. The corresponding crystal orientations of the three coordinate axes are $X=[11\bar{2}]$, $Y=[\bar{1}10]$ and $Z=[\bar{1}\bar{1}\bar{1}]$, respectively . It has been shown experimentally that the deformation twin lamellae thickness is in nanoscale. Thus, a representative twin lamella having a thickness $l_t = l_g/10$ is introduced at the center of the grain.

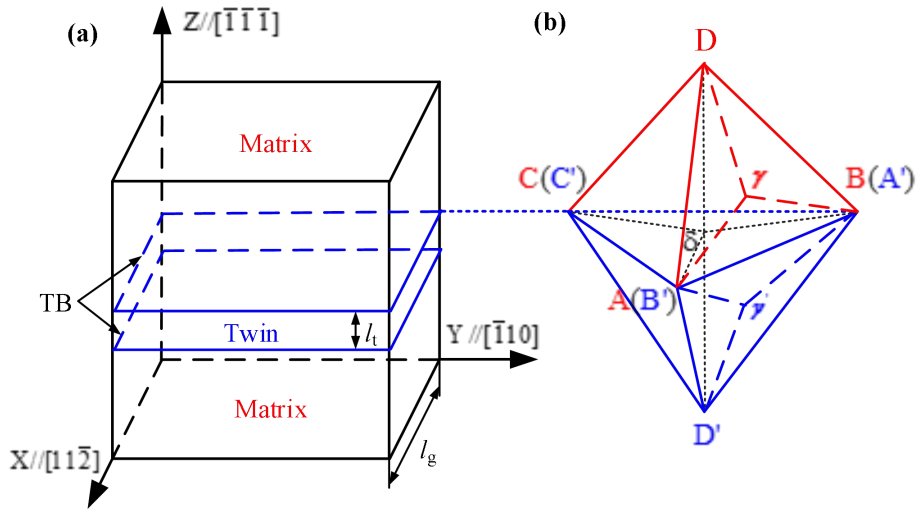

Fig. 1. (a) Schematic of the simulation cells containing the twin. (b) A double Thompson tetrahedron, the upper and lower tetrahedron represent the matrix and twinned region, respectively.

When a dislocation reaches the TB, a long and straight dislocation segment is formed at the intersection line of the slip plane and the TB. According to the angular relationship

between dislocation line and Burgers vector, as shown in Fig.1, only two types of lattice dislocations need to be considered in FCC structure. They are (a) a perfect screw dislocation with the Burgers vector parallels to dislocation line (e. g. AB on ABD plane, AC on ACD plane, BC on BCD plane); and (b) a perfect 60^{o} dislocation with a 60^{o} angle between the dislocation line and the Burgers vector (e.g. DA and DB on ABD plane, DA and DC on ACD plane, DB and DC on BCD plane). Thus, the dislocation reactions at the TB are determined by both the dislocation type and the applied stress direction. In the following sections, the possible reactions are determined for the two types of dislocations at the TB (Choi et al., 2018; Idrissi et al., 2010; Zhu et al., 2011).

2.2.1. Reactions of screw dislocation at TB

According to the previous experimental observations and MD simulation (Idrissi et al., 2010; Jin et al., 2006; Zhu et al., 2011), when a screw dislocation moves to the TB, it can either slip into the twin plane or transmit into twinned regions depending on the direction of the maximum resolved shear stress. Assuming that a screw dislocation AB on the ABD plane moves to the TB, it can be dissociated into two Shockley partial dislocations $A\delta$ and δB slipping on the ABC plane or into the $A'B'C'$ plane in the twinned region, and the dislocation reactions are designated as follows:

$$AB \rightarrow A\delta + \delta B \tag{4}$$

$$AB \rightarrow B'\gamma' + \gamma'A'(B'A') \tag{5}$$

As for the dislocation reaction in Eq. (5), a screw dislocation can glide onto the twinned region in the form of perfect dislocation without dissociation in high SFE materials such as Cu, which is similar to screw dislocation cross slip (Wei et al., 2019). However, the screw dislocation is more likely to be dissociated into two Shockley partial dislocations for TWIP steel with lower SFE. Moreover, Choi et al. (2018) observed the transmission of partial

dislocations through coherent TB by using TEM in TWIP steel micropillar. Therefore, the screw dislocation will be dissociated into two Shockley partial dislocations when it is transmitted into the twinned region in this work. The reactions of the screw dislocation at the TB are shown in Fig. 2.

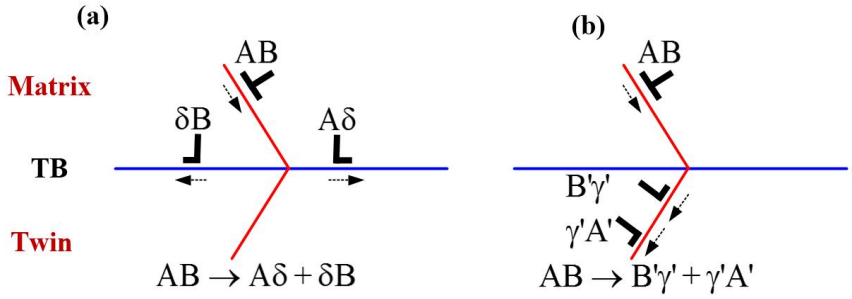

Fig. 2. Schematic of the screw dislocation reactions at TB: (a) slip into the twin plane or (b) slip into the twinned region.

2.2.2. Reactions of 60° dislocation at TB

A great number of MD simulations have been done and shown that the 60° dislocations interact with the TB in different ways depending on the material and the applied stress. The 60° dislocations can be dissociated into different partial dislocations (e.g. Shockley, stair-rod and Frank partial dislocation) transmitting into the twinned region or slipping into the TB (Jin et al., 2008; Jin et al., 2006; Wu et al., 2009). As for a 60° dislocation DA on the ABD plane moving to the TB, all the possible dislocation reactions are listed as follows (Zhu et al., 2011):

$$DA \rightarrow DB + BA \tag{6}$$

$$DA \rightarrow 2\delta A + AD' \tag{7}$$

$$DA \rightarrow BD' + C\delta \tag{8}$$

$$DA \rightarrow CD' + B\delta \tag{9}$$

$$DA \rightarrow D\delta + \delta A \tag{10}$$

According to the 60º dislocation reactions at TB denoted in Eqs. (6) to (9), a perfect dislocation can be produced after dissociation. However, the real-time observation of the dislocation-TB interactions is impractical due to the lack of efficient and available experimental techniques. It is thus difficult, if not impossible, to validate whether the perfect dislocation is produced before or after the dissociation reaction by experimental characterization. Meanwhile, despite of the fact that MD simulation can reveal the real-time evolution process of the dislocation dissociation at the TB, it would not accurately represent the reaction due to the actual loading strain rate much lower than that used in the MD simulation. All these factors make it difficult to determine the reaction results of the 60º dislocation at the TB.

To confirm the possibility and the sequence of the above reactions described by Eqs. (6) to (10), the critical resolved shear stresses (CRSS) need to be determined for the 60º dislocation reactions at the TB. From the energy point of view, it is thus believed that the above reactions occur only when the total energy before the reaction is larger than that after the reaction (Li et al., 2009). Meanwhile, the SFE is not considered in the twin growth process of TWIP steels (Guo et al., 2017; Liang et al., 2017). Based on this assumption, the following energy inequality is thus established:

$$\tau b_0^2 + 0.5\mu b_0^2 \geq 0.5\mu b_t^2 + 0.5\mu b_r^2 \tag{11}$$

where the first term on the left side of Eq. (11) represents the energy associated with the applied stress, while other three terms denote the elastic energy of per unit length for the initial dislocation and the others dislocations produced by the dissociation reaction, respectively. τ is the resolved shear stress, μ is the shear modulus. b_0, b_t and b_r represent the magnitude of Burgers vector for initial dislocation and the other dislocations

produced by the dissociation reaction, respectively. Then the CRSS τ_{crss} for the dislocation reaction at TBs is determined as:

$$\tau \geq \tau_{crss} = (0.5\mu b_t^2 + 0.5\mu b_r^2 - 0.5\mu b_0^2)/b_0^2 \tag{12}$$

Therefore, the τ_{crss} for the 60º dislocation reactions designated in Eqs. (6) to (10) are about: 32.5 GPa, 22 GPa, 11 GPa, 11 GPa and 0 GPa. In general, the tensile strength of TWIP steel is not larger than 2GPa, while the τ_{crss} for the reaction in Eqs. (6) to (9) far exceeds the tensile strength. It means that the material may have failed before the 60º dislocation reactions represented in Eqs. (6) to (9). Meanwhile, Idrissi et al. (2010) and Mahato et al. (2017) observed a large number of sessile Frank partial dislocations at the TBs by TEM and the dislocation reaction in Eq. (10) was proven by the experiment and calculation results. Thus, a perfect 60º dislocation is dissociated into a sessile Frank partial dislocation and a Shockley partial dislocation into the twin plane. The detailed dislocation reaction process is schematically illustrated in Fig. 3.

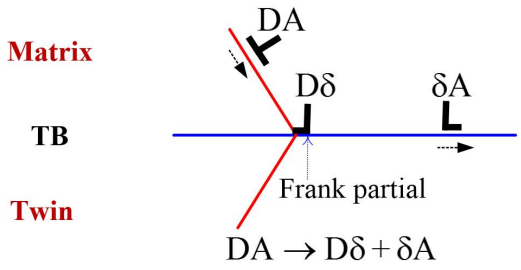

Fig. 3. Schematic of the 60 º dislocation-TB interactions.

2.2.3. Reactions of sessile Frank partial dislocation at TB

Upon the 60º dislocation dissociation denoted in Eq. (10), a sessile Frank partial dislocation occurs at the intersection line of the primary slip and twin plane. It is worth noting that the sessile Frank partial dislocation located at the interface can be further dissociated into

a sessile stair-rod dislocation and a Shockley partial dislocation (Idrissi et al., 2010; Liang et al., 2017). According to Eq. (12), the dislocation reaction is energetically favorable ($\tau_{crss} = 0$ MPa) and the Frank partial dislocation is relaxed after dissociation. Assuming that a sessile Frank partial dislocation $D\delta$ located at the intersection line of the slip plane ABD and twin plane ABC, driven by a very small stress, it can dissociate into a sessile stair-rod dislocation $\gamma\delta$ (or $\delta\gamma'$) located at the intersection line and a Shockley partial dislocation $D\gamma$ into the ABD plane or $\gamma'D'$ into the $A'B'D'$ plane depends on the direction of the maximum resolved shear stresses, as shown in Fig.4. The dislocation reactions are designated as follows:

$$D\delta \rightarrow D\gamma + \gamma\delta \tag{13}$$

or

$$D\delta \rightarrow \delta\gamma' + \gamma'D' \tag{14}$$

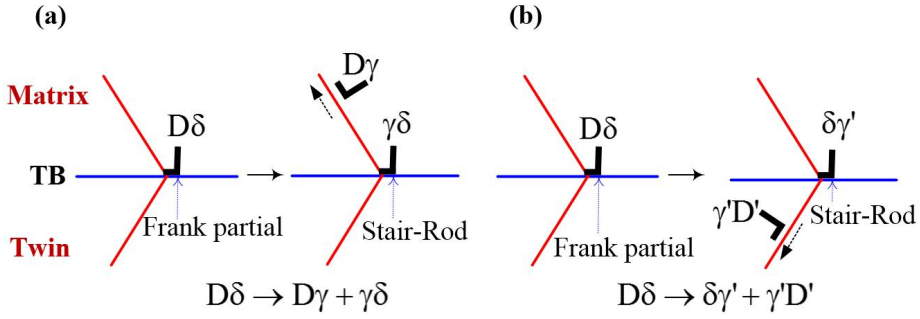

Fig. 4. Schematic of a sessile Frank partial dislocation dissociated into a sessile stair-rod dislocation and a Shockley partial dislocation (TD): the TD slips into (a) the matrix region or (b) the twined region.

2.3. Topological changes of the dislocation-TB interactions

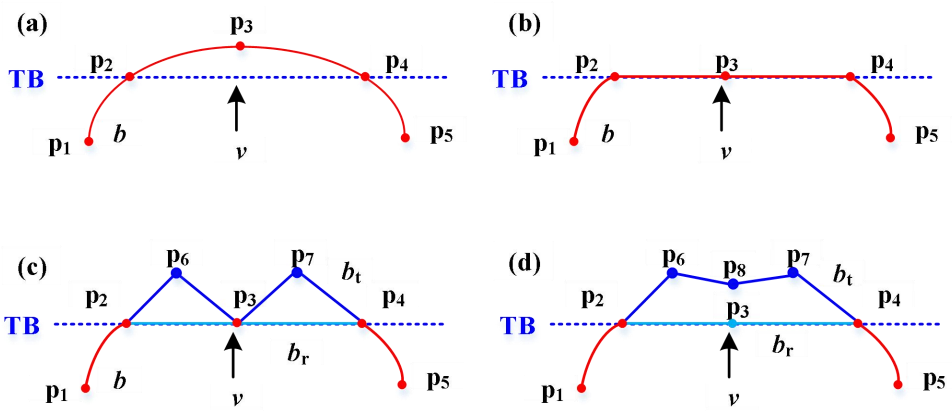

Fig. 5. Schematic of topological changes in the dislocation-TB interactions: (a) Dislocation crosses the TB. (b) Pull back to the TB. (c) Dissociated into two partial dislocations. (d) Split dislocation node p_3 into p_3 and p_8.

In DDD simulation, it is essential to deal with topological changes, i.e. the change in the node connectivity, to be faithful to the physics nature of the dislocation behavior. Fig.5 shows the detailed topological changes for the dislocation-TB interactions. When a dislocation on the slip plane inclined to the twin plane moves towards the TB, some dislocation segments (e.g. p_2p_3 and p_3p_4) may cross the TB during an integration step, as shown in Fig. 5(a). In fact, the dislocation cannot transmit the TB freely on the primary slip plane. The crossed nodes are thus pulled back to the intersection line of the slip plane and the twin plane, as shown in Fig. 5 (b). The dislocation is then dissociated into different partial dislocations based on the dislocation type and applied stress direction, as discussed in Section 2.2. Meanwhile, the Burgers vector and the slip plane of the partial dislocations produced by the dissociation reaction are changed. The dissociation reaction process is shown in Fig. 5 (c). Finally, since the node p_3 has four neighbors after dissociation, the dislocation node p_3 is split into p_3 and p_8 depending on the principle of Burgers vector conservation and the largest power dissipation as shown in Fig. 5 (d) (Arsenlis et al., 2007; Ziegler and Wehrli,

1987). It should be pointed out that, the vertical distances of nodes p_6 and p_7 to the segment p_2p_4 are set to be three times the annihilation distance in the program, to avoid merging reaction of the partial dislocations produced by the dissociation. In the subsequent DDD simulation in Section 4, the red, blue, cyan and black lines in dislocation configuration represent the perfect, Shockley partial, Frank partial and stair-rod dislocation, respectively.

3. Dislocation density-based model coupling discrete dislocation plasticity

3.1. Dislocation density-based physical model

Based on the previous studies, the evolution of the total dislocation density for a slip system i accounts for the multiplication of dislocations (Allain et al., 2004), the mutual annihilation for closely spaced dislocations of opposite sign, i.e. dynamic recovery of dislocation, and the escape of the dislocations through free surface for the TWIP steel micropillar with the free surface (Cui et al., 2014), it can be written as:

$$\frac{\mathrm{d}\rho^{(i)}}{\mathrm{d}\gamma^{(i)}}=\frac{1}{b\Lambda^{(i)}}-\frac{y}{b}\rho^{(i)}-\frac{2}{bD} \tag{15}$$

where $\rho^{(i)}$ is the dislocation density for the slip system i, $\gamma^{(i)}$ is the plastic shear rate on the slip system i, $\Lambda^{(i)}$ is the MFP that the dislocation can move along before storage, y is a parameter associated with the dynamic recovery and set to be 10^{-9} m (Lu et al., 2020), D is the effective grain size.

In the present model, the MFP is calculated with a harmonic mixing law accounting for the GBs, TBs and the forest dislocation (Allain et al., 2004). For the TWIP steel micropillar with the free surface, the TB and the forest dislocation are introduced to describe the MFP for a given slip system i, the MFP then becomes:

$$\frac{1}{\Lambda^{(i)}}=\frac{1}{T^{(i)}}+K_1\sqrt{\rho} \tag{16}$$

where $T^{(i)}$ represents the spacing between the twins secant to the slip system i, K_1 is a dimensionless constant and set to be 10^{-2} (Allain et al., 2004). The second term on the right side in Eq. (16) can be considered as the characteristic length of the Frank-Read (FR) source in the forest dislocations and it reflects the effect of the forest dislocation on the FR source (Cui et al., 2014). ρ denotes the sum of the dislocation density of 12 slip systems, i.e. $\rho = \sum_{i=1}^{12} \rho^{(i)}$.

The effect of twin spacing on the MFP of dislocation is given as:

$$\frac{1}{T^{(i)}} = B_{ij} \frac{1}{t_j} \tag{17}$$

where B_{ij} represents the dislocation-TB interactions matrix defined using the following rules: $B_{ij} = 0$ if slip system i and the twinning system j are coplanar; while $B_{ij} = 1$ if slip system i and the twinning system j are secant. t_j is the distance between two twin stacks of a given twinning system j, which is calculated using a modified Fullman's stereological relationship to account for multi twin systems (Allain et al., 2004):

$$\frac{1}{t_j} = \frac{f_{\mathrm{t}}^{(j)}}{2e\left(1 - \sum_{j=1}^{12} f_{\mathrm{t}}^{(j)}\right)} \tag{18}$$

where e is the mean thickness of the twin and generally set at 30 nm, $f_{\mathrm{t}}^{(j)}$ is the twin volume fraction of twinning system j.

The shear rate of slip system i can be obtained directly by the power-law flow rule and has the following form (Li et al., 2014):

$$\dot{\gamma}^{(i)} = \dot{\gamma}_0 \left| \frac{\tau^{(i)}}{\tau_s^{(i)}} \right|^{\frac{1}{m}} \mathrm{sign}(\tau^{(i)}) \tag{19}$$

where, $\tau^{(i)}$ is the resolved shear stress on the slip system i, $\tau_s^{(i)}$ is the slip resistance for the slip system i, $\dot{\gamma}_0$ is a reference shear rate which is taken to be the same for all the slip systems and set at 0.001 s^{-1} (Sun et al., 2016), m is the strain rate sensitivity parameter and set at 0.02.

Based on the generalized size-dependent Taylor-strengthening law, the slip resistance under the different mechanism regions (i.e. dislocation starvation, activation of a single source, exhaustion hardening, forest strengthening) can be identified by the dislocation density (El-Awady, 2015). Meanwhile, the back stress term $\tau_{\mathrm{b}}^{(i)}$ is introduced due to the dislocation pileups at the TB. Thus, the critical resolved shear stress for a slip system i is expressed as:

$$\tau_{\mathrm{s}}^{(i)} = \tau_0 + \alpha\mu b\sqrt{\rho} + \frac{\beta\mu}{D\sqrt{\rho}} + \tau_{\mathrm{b}}^{(i)} \tag{20}$$

where τ_0 is the lattice friction stress and set at 78 MPa (Liang et al., 2016), α and β are material constant. α is generally set to be 0.5 and β is taken as 10^{-3} in previous researches (El-Awady, 2015). $\tau_{\mathrm{b}}^{(i)}$ is the back stress for slip system i.

The second term in Eq. (20) is the traditional forest-strengthening term which states that the dislocation MFP is inversely proportional to the square root of the dislocation density when $\alpha b\sqrt{\rho} >> \beta/D\sqrt{\rho}$, which can also be considered as the effective source length λ in the forest dislocations (El-Awady, 2015),

$$\lambda \propto 1/\sqrt{\rho} \tag{21}$$

On the other hand, when $\alpha b\sqrt{\rho} << \beta/D\sqrt{\rho}$, the forest hardening term becomes negligible and the strength is mainly governed by the resolved shear strength required to

activate the weakest dislocation sources. The dislocation source strength is proportional to the inverse of the effective source length λ , i.e. the third term in Eq. (20), and the effective dislocation source length should be given by (El-Awady, 2015):

$$\lambda \propto bD\sqrt{\rho} \tag{22}$$

According to the classical dislocation pileup theory, the local resolved back stress acting on a given dislocation source depends on the trapped dislocation density (Bouaziz et al., 2011). The back stress caused by the TB linearly depends on the dislocation density in the following (Cui et al., 2015):

$$\tau_{\mathrm{b}}^{(i)} \approx \alpha^{'} \mu b D \rho^{(i)} \tag{23}$$

where, $\alpha^{'}$ is a dimensionless constant.

3.2. Coupling procedure between the DDD and DDB model

In the above DDB model, just the angular relationship between the twin plane and slip plane is considered in describing the dislocation-TB interactions. As shown in Fig.6 (a), the dislocation-TB interactions matrix $B_{ij} = 1$ when the slip plane and the twin plane are secant. In this case, the TB is treated as the GB and has a high resistance to the dislocation slip. However, a large number of experimental observations and MD simulations (Idrissi et al., 2010; Jin et al., 2006; Liebig et al., 2018; Zhu et al., 2011) revealed that the dislocation reactions at the TBs should also be considered in describing the resistance of the TB to the dislocation slip. Because the dislocation can cross slip into the twin plane (absorbed), transmit into the twinned regions or be blocked by the TB, depending on the dislocation type and the applied stress, as shown in Fig.6 (b). To accurately represent the dislocation-TB interactions, matrix B_{ij} in DDB model and the dislocation reactions at the TB are systematically discussed by DDD simulations in the following sections.

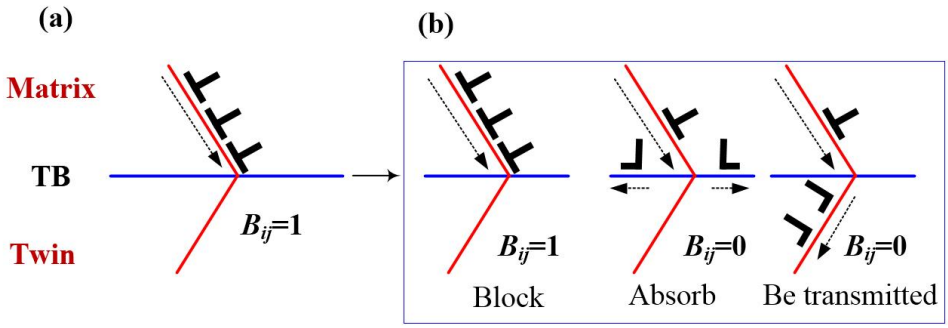

Fig. 6. (a) Schematic of the resistance of the TB to dislocation slip in DDB model. (b) The dislocation reactions at the TB in DDD.

3.3. Simulation setup

The DDD simulations were performed by using the DDLab code developed by Cai and colleagues (2013), which runs in a Matlab environment. In the present DDD simulation, the cubic cell has the grain size of l_g=1μm . Initially, equal amounts of Frank-Read (FR) dislocation sources are distributed to all slip systems, ensuring all slip systems to be equally treated for activation. The position and the orientation of FR sources are randomly distributed. It needs to point out that the FR sources are just distributed in the matrix region since the deformation twin lamellae thickness is in nanoscale and the dislocation in the twinned region is difficult to be activated. The source lengths are randomly distributed from 200 to 300 nm, and the initial total dislocation density ρ_0 is about 10^{12} m^{-2}. Others material properties are as follows: shear modulus μ is 65 GPa (Bouaziz et al., 2011), Poisson's ratio ν is 0.31, Burgers vectors for perfect, Shockley, stair-rod and Frank partial dislocation are 0.256, 0.147, 0.085 and 0.208nm, respectively. Uniaxial tension is applied to the sample with various loading angles (θ) to the Z axis including perpendicular ($\theta = 90^\circ$, Y axis), parallel ($\theta = 0^\circ$, Z axis) and inclined ($\theta = 45^\circ$, YZ). A strain rate of 5000 s^{-1} is imposed to attain a higher computing efficiency (Fan et al., 2015). Here, a cut-off plastic strain rate is introduced, e.g. the stress keeps constant when the plastic strain rate is larger than 5000 s^{-1}, such that the

applied loading does not decrease (Cui et al., 2014).

In the DDB model, the grain shape and crystallographic orientations are identical to the DDD model for the sake of the comparison study. First, given the initial dislocation density ρ_0 for all slip systems and twin volume fraction f_0 in ABC plane, the mean distance between two twin stacks and the initial slip resistance can be estimated by Eq. (18) and (20), respectively. In calculations, the strain rate $\dot{\varepsilon}$ is the input and the stress σ update is calculated by $\mathrm{d}\sigma = E \cdot (\mathrm{d}\varepsilon - \mathrm{d}\varepsilon_{\mathrm{p}})$, where E and $\mathrm{d}\varepsilon_{\mathrm{p}}$ are the elastic modulus and the plastic strain increment, respectively. The slip shear rate $\dot{\gamma}$ can be obtained according to Eq. (19). The resolved shear stress τ and the plastic strain increment $\mathrm{d}\varepsilon_{\mathrm{p}}$ are calculated according to the Schmid's law. Meanwhile, the next step's dislocation density ρ is updated according to the current dislocation density by the statistical model in Eqs. (15) to (18). The critical resolved shear stress τ_{s} is finally calculated by Eqs. (20) to (23).

4. Simulation results and discussion

4.1. The effect of TB orientation in DDD

The stress-strain curves and the dislocation density evolution during the tension process are plotted in the same graph for TWIP steel single and the twinned crystal micropillars with different loading directions, as shown in Fig. 7(a). For the TWIP steel single crystal, the yield stress under different loading directions has an obvious orientation effect due to the different Schmid factors. Compared with the available experimental results given in Fig. 7(b) for the TWIP steel micropillar with the diameter D=1μm , the DDD simulation results of yield stress agree with the experimental results obtained by Choi et al. (2017) and Wang and Stanford (2017). In the later part of the stress-strain curves, the flow stress keeps almost constant with the ongoing deformation without any obvious strain hardening. As for the

dislocation density in Fig. 7(a), it keeps at a low level, fluctuates around a constant value for all loading directions. The emergence of many peaks in the dislocation density curves means that the propagation rate by FR source and the escape rate from the free surface is balanced. However, comparing with the yield stress of TWIP steel single and twinned crystal micropillar, it can be seen that the yield stress, strain hardening rate and dislocation density for the twinned TWIP steel are increased rapidly along the 0º direction. This is consistent with the experimental results of the nanotwinned Cu loading at the same orientation (You et al., 2013). While the mechanical response changes little when the tension oriented at 45º and 90º compared with the TWIP steel single crystal, the same trend of flow stress is observed in the comparison test for the TWIP steel twinned crystal micropillar with the diameter D=4μm (Choi et al., 2018), as shown in Fig.7(b). The above results indicate that the twins have an obvious orientation effect on the plastic deformation behavior of TWIP steels.

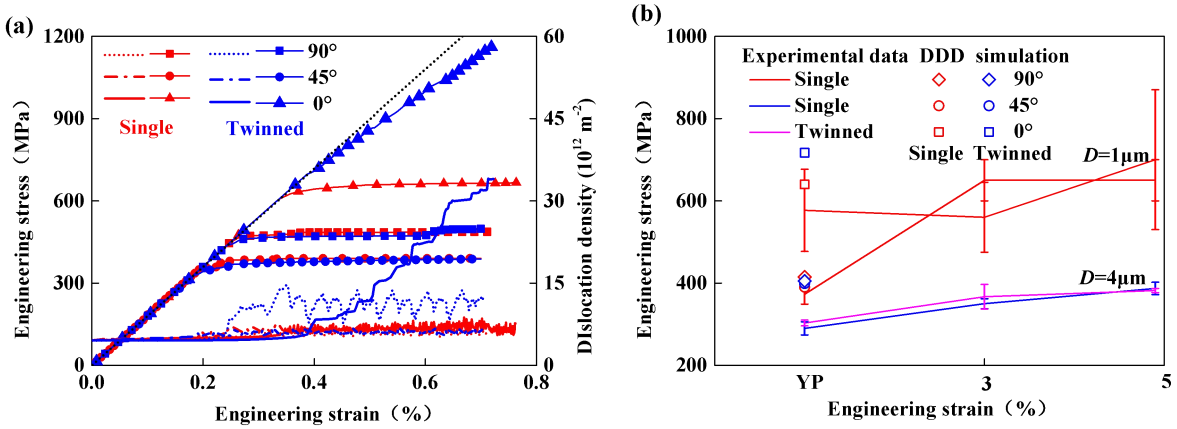

Fig.7. (a) Engineering stress and dislocation density-strain curves for single and twinned crystal during tension oriented at 0 º, 45º and 90º (The black dotted line reflects the purely elastic response). (b) Comparison the yield stress between DDD simulation and experiment result. Statistical comparison of stresses at the yield point (YP) and at engineering strain levels of 3% and 5% for TWIP steel micropillar with a diameter 4 μm (Choi et al., 2018) and 1 μm (Choi et al., 2017; Wang and Stanford, 2017).

To further reveal the influence of deformation twins on dislocation evolution, Fig.8 shows the corresponding dislocation microstructures for the twinned TWIP steel crystal along different directions with respect to the TB at the strain of 0.7%. It is observed that the screw FR sources on the slip plane inclined to the TB are activated along 90º tension (Y axis). In this case, the screw dislocation dissociated into two Shockley partial dislocations (b_t) and transmitted into the mirror plane in the twinned region by cross slip, as shown in Fig.8 (a). The screw FR sources are thus continuously activated and transmit the TB to accommodate the plastic deformation without increasing stress. In the 45º tension case, the dislocations on the slip plane parallel to the twin plane with the maximum Schmid factor of 0.44 are activated, as shown in Fig.8 (b). It is consistent with the experiment test and MD simulation results for the nanotwinned Cu in oriented at 45º done by You et al. (2013). In this case, the TB does not affect stress-strain and dislocation density evolution, which is the same as the mechanical response of TWIP steel single crystal shown in Fig.7. When the loading is 0º tension (Z axis), the 60 º FR sources on the three slip planes DAB, DAC and DBC (see Fig. 8(e)) inclined to the TB are all activated due to the same Schmid factors (0.27). The activated FR sources are impeded and form a long, straight dislocation segment at the intersection line slip plane and the TB. It is noted that both the resolved shear stress and the Schmid factor of the twin plane are 0 when the loading direction is perpendicular to the TB. Thus, the dislocation pileups are expected with the increasing number of dislocations moving towards the TB and the interactions between dislocation-dislocation are shown in Fig.8(c) and (e). As a result, the applied stress must be increased intermittently to continuously activate the FR source, resulting in the increase of yield stress and high strain hardening rate. With the increase of dislocation pileups, the shear stress acting on the leading 60º dislocation increases remarkably, thus the leading 60º dislocation is dissociated into a sessile Frank partial dislocation (b_F) and a Shockley partial dislocation (b_t) slipping on TB under the interaction

of other 60º dislocations. Furthermore, the sessile Frank partial dislocation is dissociated into a sessile stair-rod dislocation ($b_{s\text{-}r}$) at the intersection line of slip plane and the TB, the Shockley partial dislocation is transmitted into the twinned region, as shown in Fig.8(d). The sessile Frank partial dislocation and stair-rod dislocation also block the movement of the subsequent dislocations to the TB. Therefore, the twins play an important role in strain hardening when the loading direction is perpendicular to the TB. The above DDD simulation results show the dislocation-TB interactions as a function of the dislocation type and loading directions for TB (Liebig et al., 2018).

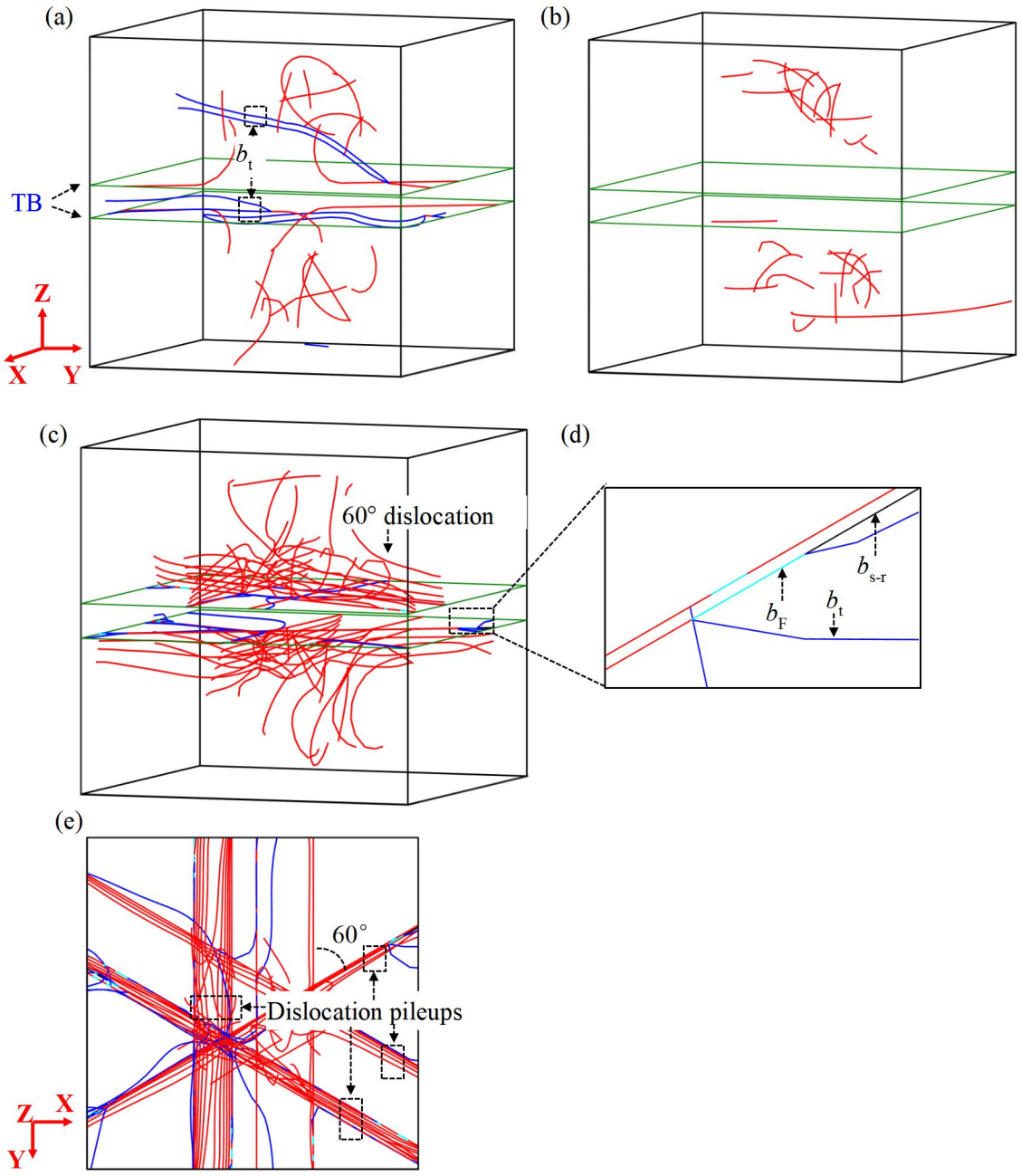

Fig.8. Dislocation microstructure for twinned TWIP steel crystal under different tension directions: (a) 90º, (b) 45º, (c) 0º. (d) The enlarged image of the areas marked by squares in (c), which shows dislocation-TB interactions details and (e) the vertical view of 0º direction.

4.2. Individual dislocation reaction at TB

In the above DDD simulation, the strain value is relatively small due to the limited computation capacity. When the flow stress reaches a high value with the increasing strain during the loading process for TWIP steel polycrystalline, different types of dislocations with the high applied stress are activated to interacts with the TB and affect the macroscopic plastic behavior. In order to exactly reveal the influence of the twin on the dislocation slip and avoid the interaction of dislocations with the activation of multiple FR sources, the influence of twins on flow stress and hardening behavior is analyzed intuitively. The activation evolution of an individual FR source on different slip plane and its interaction with the TB under different loading directions are discussed in the following.

Fig. 9 shows the evolution results of flow stress, dislocation density and corresponding dislocation configurations for an individual screw and 60º FR source in ABD plane under tension oriented at 90º (Y axis). It is observed that the mechanical behavior is dominated by dislocation type as shown in Fig.9 (a), for the screw dislocation, the flow stress almost keeps constant, and the dislocation density curves fluctuate near a constant value with ongoing deformation without strain hardening after yield point. It can be seen from the dislocation configuration in Fig.9 (b) that the screw dislocation is dissociated into two Shockley partial dislocations and transmits into the mirror slip plane in the twinned region when it reaches the TB1. The leading Shockley partial dislocation is impeded when it moves to the TB2 until the trailing partial dislocation is also moving to the TB2. Then the leading and trailing partial dislocations merged to form a perfect screw dislocation at TB2. Further, the perfect screw dislocation is dissociated again and transmits the TB2 until it escapes from the free surface. Therefore, the stress and dislocation density reach the stable value due to the screw dislocation propagating, transmitting TB and escaping from free surface.

While as for the 60º FR source, the flow stress and the dislocation density increase rapidly after yield point along the Y direction. It can be seen from the dislocation configuration in Fig. 9(c) that the dislocation pileups at the TB with the increasing number of 60º dislocations, and the 60º dislocation dissociation reaction at TB is same to the loading along Z axis as shown in Fig.8(c). By observing the mechanical behavior and microstructures corresponding to 60º dislocation loading along Y and Z axis, it can be found that the sessile Frank partial dislocation and stair-rod dislocation produced by 60º dislocation dissociation, which will hinder the subsequent dislocations moving to the TB. Therefore, the result indicates that 60º dislocation pileups dominate the stress increase and strain hardening.

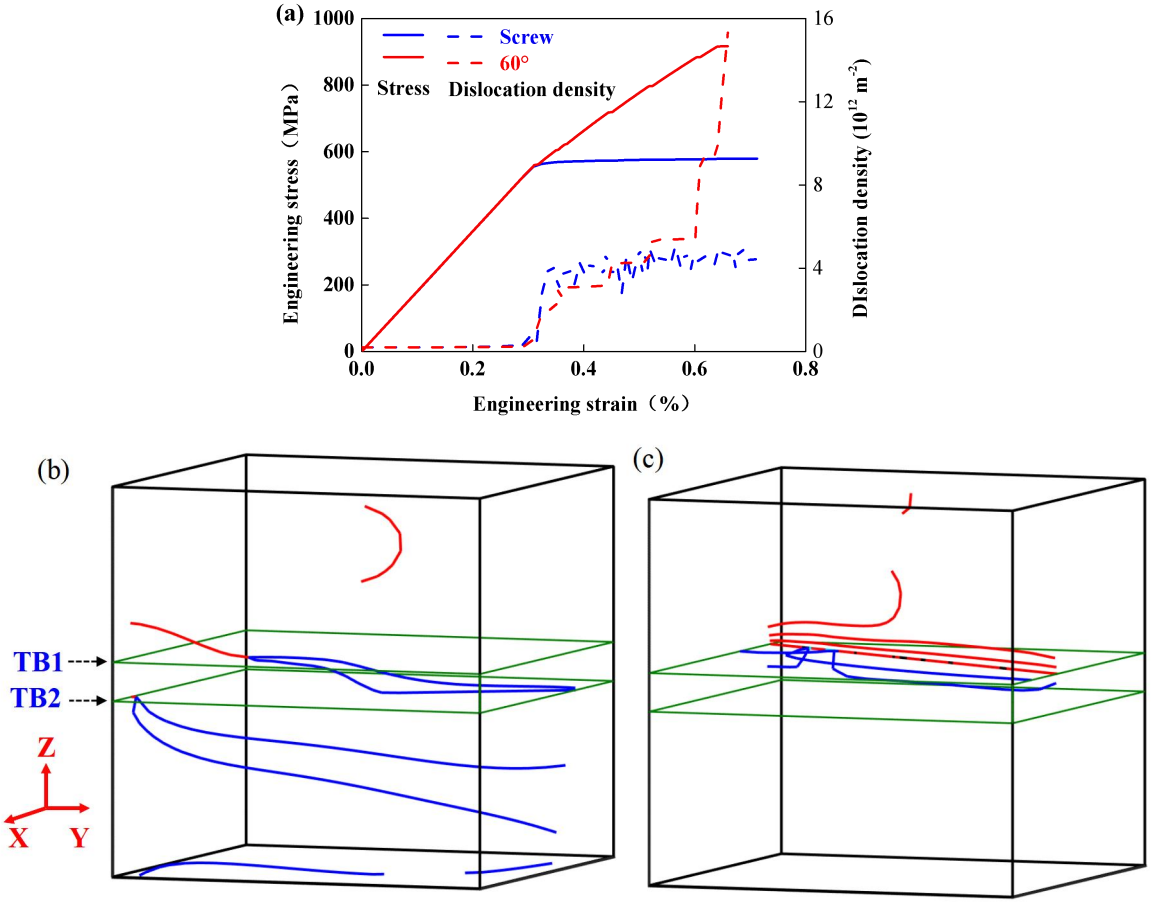

Fig.9. (a) Stress and dislocation density-strain curve for screw and 60º FR source in ABD plane under tension oriented at 90º. (b) Dislocation microstructure after loading for the screw dislocation. (c) Dislocation configuration after loading for the 60º dislocation.

Fig.10 shows the evolution of mechanical behaviors and dislocation configurations after loading for the individual screw FR source in BCD and ABD plane along the 45º direction. It is observed that the strain hardening keeps low after the yield point for screw dislocation in both planes, while the dislocation density is different obviously, as shown in Fig. 10 (a). For the screw dislocation on BCD plane, as shown in Fig.10 (b), dissociates into two Shockley partial dislocations at TB and cross slips onto the twin plane. In this case, the two Shockley partial dislocations slip in the same direction to accommodate the plastic deformation without increasing stress and dislocation density. While the flow stress remains almost a constant and the dislocation density increase rapidly after yield point for the screw dislocation on ABD plane, the dislocation network configuration appears on the twin plane as shown in Fig.10 (c).

Further details about the formation process of the dislocation network configuration are shown in Figs.10 (d)-(g). Fig.10 (d) shows that the screw dislocation is dissociated into two Shockley partial dislocations and move in the opposite direction on the TB, which results in the twin growth or de-twinning. Meanwhile, the Shockley partial dislocations (e.g. b_{t1} and b_{t2}) in Fig.10 (e) gradually change to the screw dislocation orientation under the action of line tension, the two Shockley partial dislocations cannot keep paralleling with the increase of distance. By observing the microstructures corresponding to this stage, the subsequent screw dislocations is also dissociated into Shockley partial dislocations on the adjacent twin planes when they slip to the TB as shown in Fig. 10(f). In this way, many Shockley partial dislocations interact on the adjacent twin planes, resulting in the final formation of dislocation network configuration, as shown in Fig. 10(g).

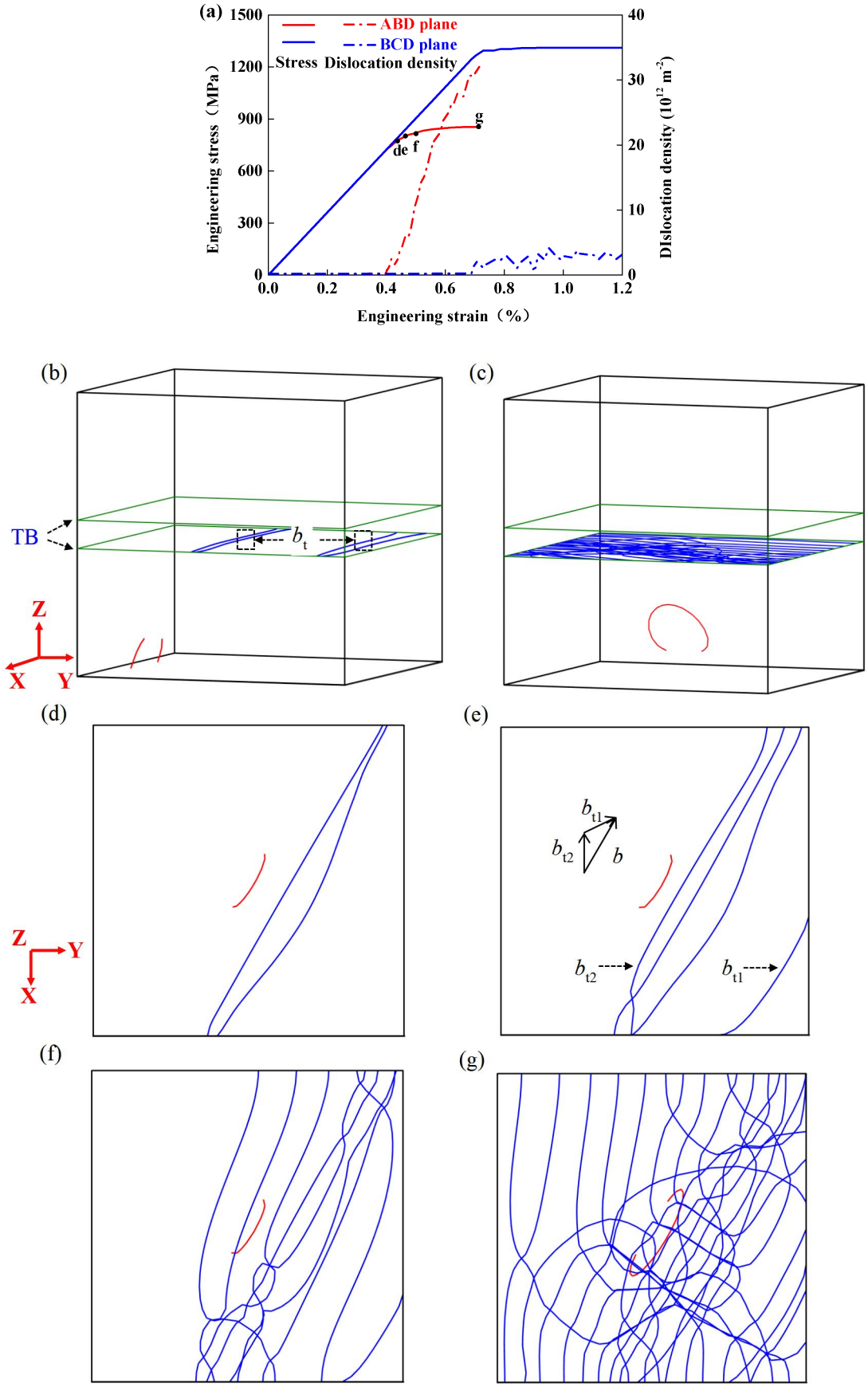

Fig.10. (a) Stress-strain and dislocation density-strain curve for screw FR source in ABD and

BCD plane under tension along 45º direction. The marked points correspond to the dislocation configurations in (d-g). (b) Dislocation configuration for the screw dislocation in BCD plane. (c) Dislocation microstructure for the screw dislocation in ABD plane. (d-g) Snapshots of configurations for the screw dislocation in ABD plane during tension.

Fig.11 shows the evolution of mechanical behaviors and dislocation configurations after loading for the individual 60º FR source in the BCD plane under tension along the Z direction. It is observed that the simulation results are similar to the results with a complex dislocation configuration. The dislocations are trapped and pileup at the TB with the increasing number of 60º dislocations, as shown in Fig.11 (b). With the increasing of 60º dislocation pileups, the shear stress acting on the leading 60º dislocation along the TB increases remarkably. Thus, the leading 60º dislocation is dissociated into a sessile Frank partial dislocation (cyan line) and a Shockley partial dislocation (blue line) slipping on TB. The sessile Frank partial dislocation and stair-rod dislocation can also block the subsequent dislocations moving toward the TB. In this condition, the stress is required to increase to remobilize the FR source intermittently, leading to high strain hardening rate close to the elastic modulus as shown in Fig.11 (a). Meanwhile, after the dislocation dissociation, the total dislocation density and the trapped dislocation density are also gradually different.

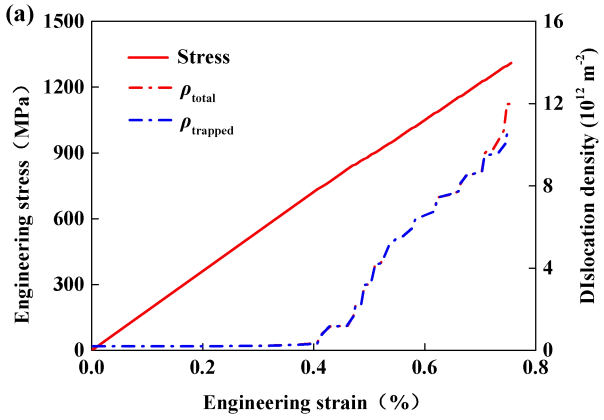

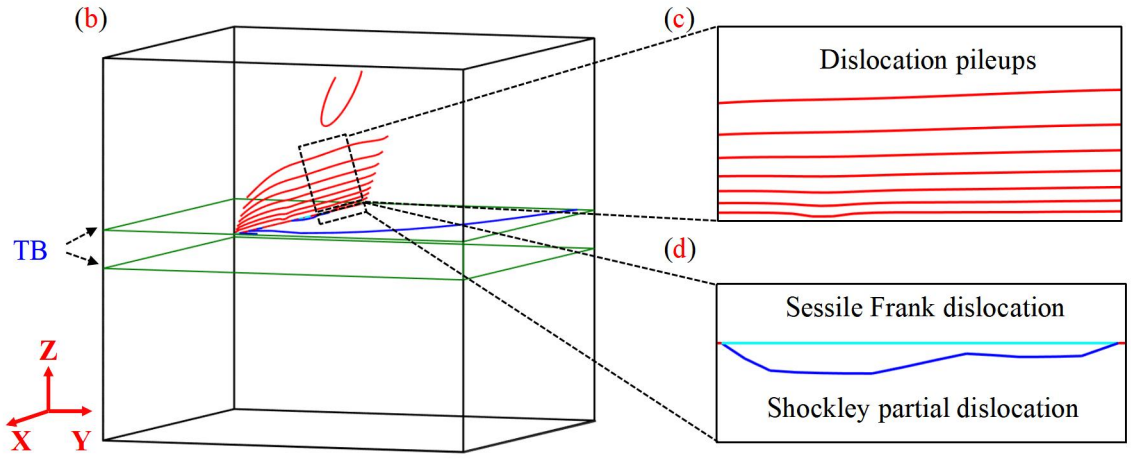

Fig.11. (a) Stress, total dislocation density and trapped dislocation density-strain curve for micropillar containing individual 60º FR source in BCD plane under tension along Z direction. (b) Dislocation configuration after loading. (c, d) The enlarged image of the areas marked by squares in (b), which show the dislocation pileups and the dissociation reactions, respectively.

4.3. Improvement of the DDB model and predicting the TB orientation effect

The above DDD simulation results are valid for the isotropic elastic cases. It is found that the TB just blocks the 60º dislocation and has no influence on the screw dislocation. Therefore, both the angular relationship between the incoming dislocation slip planes and the TB plane proposed by Allain et al. (2004) and the dislocation type in describing the dislocation-TB interactions. For 60º dislocation, the TB blocks the dislocation movement increasing the flow stress, which is a hardening model. While the screw dislocation may dissociated into two Shockley partial dislocations on the TB or traverse the TB into the twinned region to accommodate the plastic deformation, which is similar to cross slip. In this section, an improved DDB model is proposed to represent the plastic behavior via taking into account the dislocation type in description of the dislocation-TB interactions in the dislocation density evolution equation. The dislocation type determination formula is proposed in the following.

The dislocation form a straight dislocation segment in the intersection line of the slip plane and the TB, the dislocation segment is perpendicular to the normal directions of both the twin plane and slip plane. As shown in Fig.12, the dislocation type can thus be determined by the following rules: It is a screw dislocation if a given twin plane normal n_j is perpendicular to the Burgers vector of the dislocation segment b_i, i.e. $\left|\cos\left(b_i, n_j\right)\right| = 0$; while it is a 60º dislocation if the angle between the normal direction for a given twin plane n_j and the Burgers vector of the dislocation segment b_i is less than 90º, i.e. $\left|\cos\left(b_i, n_j\right)\right| > 0$. The TB can only trap the 60º dislocations on the slip planes secant to the TB and the screw dislocations can cross slip into the twinned region or the twin plane. Therefore, the dislocation-TB intersections matrix B_{ij} in DDB model can be improved by incorapeting both the dislocation type and the angular relationship between the incoming dislocation slip planes and the TB plane:

$$B_{ij}^{'} = B_{ij} \cdot \mathrm{sign}\left(\left|\cos\left(b_i, n_j\right)\right|\right) \tag{24}$$

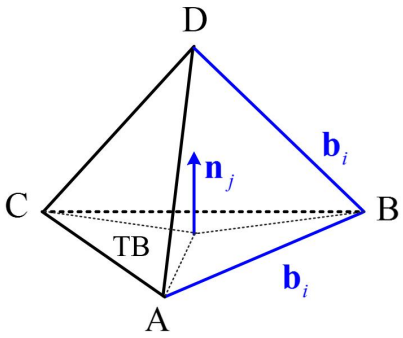

Fig. 12. Schematic of a given twin plane normal n_j and the Burgers vector of the dislocation line b_i in the Thompson tetrahedron.

Thus, the dislocation type should also be considered in describing the dislocation multiplication and escaping from the free surface, the dislocation density evolution model is

thus modified as follows:

$$\frac{\mathrm{d}\rho_i}{\mathrm{d}\gamma_i}=\frac{1}{b\Lambda_i}-\frac{y}{b}\rho_i-\frac{2\left(1-B_{ij}^{'}\right)}{bD} \tag{25}$$

The first term in Eq. (25) on the right side describing the evolution of the MFP reflects the multiplication of dislocations under the forest dislocation condition, while the activation of the dislocation sources has not yet been considered. Inspired by the dislocation multiplication term in Eq. (16) and considering the different effective dislocation source length λ of the initial stage in Eq. (22), in this research the dislocation multiplication rate by activation of the dislocation sources is introduced to represent the MFP as follows:

$$\frac{1}{\Lambda_i}=\frac{B_{ij}^{'}}{T_i}+K_1\sqrt{\rho}+\frac{K_2}{bD\sqrt{\rho}} \tag{26}$$

where the last two terms in Eq. (26) on the right side represent the dislocation multiplication under different dislocation density conditions and K_2 is a dimensionless constant with the value of 10^{-4}.

According to the classical dislocation pileup theory, the local resolved back stress acting on a given dislocation source depending on the trapped dislocation density (Bouaziz et al., 2011). Thus, the trapped dislocation density is replaced by the 60º dislocation density since only the 60º dislocations are trapped by the TB. According to the dislocation type decision method in Eq. (24), the back stress depends linearly on the 60º dislocation density in the following form (Cui et al., 2015):

$$\tau_{\mathrm{b}}\approx\alpha^{'}\mu bD\rho_i\cdot\mathrm{sign}\left(\left|\cos\left(b_i,n_j\right)\right|\right) \tag{27}$$

The relations between back stress and the trapped 60º dislocation density in Fig.11 (a) is plotted in Fig.13. It is noted that the back stress increase stepwise as the 60º dislocation

pileups. α' is about 0.75 according to the least-square fitting of simulation result.

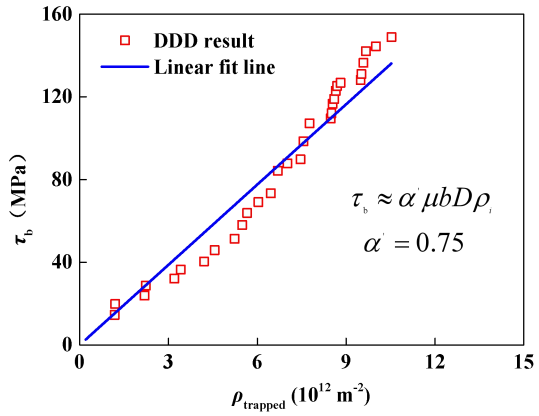

Fig. 13. The back stress-trapped dislocation density for TWIP steel micropillar.

Thus an improved DDB model is proposed by considering the dislocation type in describing the dislocation-TB intersections. In the above DDD simulation results for TWIP steel micropillar, both the twin orientation associated with loading directions and the dislocation type play a significant role in the evolution of macroscopic mechanical response. As shown in Fig.14, the stress and dislocation density-strain curve can all be predicted by the improved DDB model in this research, which show the same trend as the above DDD results for the 0º, 45º and 90º tension in Fig.7. Meanwhile, in the presented DDB model, the macroscopic stress-strain responses for FCC crystal under different angles between the twin plane normal and loading direction are also consistent with the prior DDD simulation results (Wei et al., 2019). As angles vary from 0º~15º, significant hardening is observed, which can be attributed to 60º dislocation pileups at the TB. With an increase of the angles 15º~30º, the effect of twinning on strain hardening is obviously reduced. As the angles are greater than 30º, the effect of twin on strain hardening can be ignored.

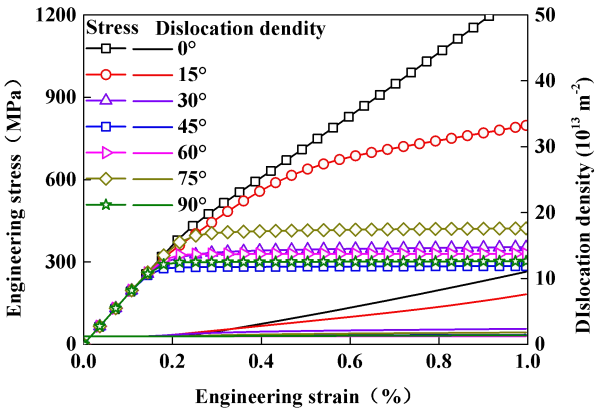

Fig. 14. Evolution of engineering stress and dislocation density-strain for twinned TWIP steel micropillar under different tension angles with respect to the twin plane normal by the improved DDB model.

It can be seen that the improved DDB model shows its ability to capture the TB orientation effect in TWIP steel micropillar. Further quantitative comparison between the DDD simulation results and the improved DDB model analysis is made and shown in Fig. 15 for revealing the TB's influence on yield stress. The yield stress from the analytical and DDD simulation results is converted into the resolved shear stress to facilitate the comparison. An excellent quantitative agreement is also obtained. For 0º tension, the increase of the yield stress is maximum. The TB's contribution to the yield stress is gradually decreased with the angles from 0º~30º and becomes negligible when the loading angle is larger than 30º.

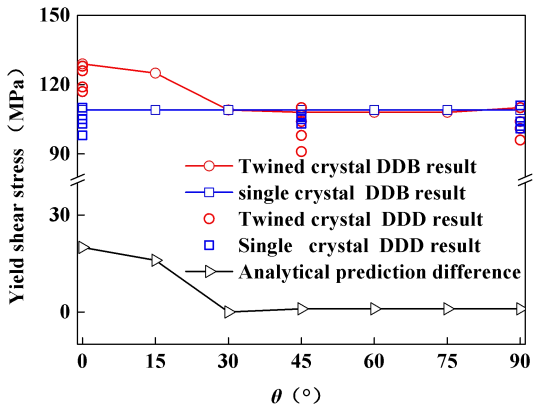

Fig. 15. Comparison between the yield shear stress for the twinned and the single TWIP steel

micropillar by the DDD simulation and the improved DDB model analysis.

According to the analysis above, both of the twin orientation and dislocation type significantly influence the stress increasing and strain hardening. The experimental results obtained prior researches showed that the deformation twin planes are inclined at a certain angle (generally at 30º~60º) in the deformation of TWIP steel (Bouaziz et al., 2011; Choi et al., 2017; Idrissi et al., 2010; Liang et al., 2017), rather than in parallel nor perpendicular to the loading direction. Based on the above results of DDD simulations and the improved DDB model analysis, the effects of deformation twins on yielding and strain hardening behaviors are limited, which is consistent with the experimental results obtained by peers (Liang et al, 2016; Luo and Huang, 2018).

5. Conclusions

(1) A new dislocation-TB interactions DDD model was developed to investigate the influence of twin on dislocations in the deformation behavior of TWIP steel. For the proposed model, the complicated dislocation reactions at the TB was determined by the energy criterion and the corresponding topology changes was formulated.

(2) The TBs exhibit a strong orientation effect on the deformation behavior of TWIP steel micropillar. The TB had a significant strengthening effect at 0º tension due to the back stresses caused by the 60º dislocation pileups. While the strain hardening effect becomes negligible for 45º and 90º tension. Furthermore, the resistance of the TBs to dislocations was related to the dislocation type, the TB just blocked the 60º dislocation and had not influence on the screw dislocation.

(3) The association between the DDD and the DDB was established by incorporating the dislocation type and reaction characteristic at the TBs in DDD into the conventional DDB model. Moreover, the dislocation type discrimination criteria applicable to DDB model was

proposed by considering the angular relationship between the twin plane normal and the Burgers vector of the dislocation in describing the dislocation-TB interactions.

(4) This improved DDB model successively predicted the evolution of stress and dislocation density-strain at different loading directions relate to the twin plane normal. The mechanical response results agreed well with the available DDD simulation and the experimental results.

(5) The TB's contribution to the yield stress and strain hardening was gradually decreased with the increase of angles between the loading direction and twin plane normal, the contribution could be negligible when the angles was larger than 30º. This result explained why the deformation twins had a limited contribution to the flow stress and strain hardening in the deformation behavior of TWIP steel.

It should be pointed out that the newly proposed dislocation-TB interaction model in DDD is limited to long straight dislocation line under low strain rate or low stress loading. Future MD simulation needs to consider the dislocation reactions with different dislocation line lengths, local curvatures, applied stresses and strain rates. In the current dislocation-TB interactions model, only twin growth (or de-twinning) is considered in DDD simulation. But twin nucleation and propagation, which play an important role in deformation twinning and the simultaneous influence of stacking faults between the two partial dislocation lines needs to be considered in future DDD research. Thus a new dislocation-TB interactions DDD model to describe the whole process of twin nucleation, propagation and growth is also needed to be established. The improved DDB or DDD model should be incorporated into the continuum crystal plasticity as a new constitutive relation to study the more complicated plastic behaviors of crystalline materials in a large scale of plastic deformation.

Acknowledgements

This work is supported by the National Natural Science Foundation of China (NSFC) (51805023), Joint Foundation of NSFC and China Academy of Engineering Physics (U1730121), China National Key Laboratory Foundation of Science and Technology on Materials under Shock and Impact (6142902180201), the International Exchanges Scheme of NSFC and Royal Society under Grant (51911530209). Wei Cai and colleagues at Stanford University are gratefully acknowledged for making the DDLab software always available for use.

References

Allain, S., Chateau, J.P., Bouaziz, O., 2004. A physical model of the twinning-induced plasticity effect in a high manganese austenitic steel. Mater. Sci. Eng., A. 387, 143-147.

Arsenlis, A., Cai, W., Tang, M., Rhee, M., Oppelstrup, T., Hommes, G., Pierce, T.G., Bulatov, V.V., 2007. Enabling strain hardening simulations with dislocation dynamics. Model. Simul. Mater. Sci. Eng. 15, 553-595.

Bouaziz, O., Allain, S., Scott, C.P., Cugy, P., Barbier, D., 2011. High manganese austenitic twinning induced plasticity steels: A review of the microstructure properties relationships. Curr. Opin. Solid State Mater. Sci. 15, 141-168.

Cai, W., Deng, J., Kang, K., 2013. A short course on DDLab and ParaDiS. http://micro.stanford.edu/~caiwei/Forum/2005-12-05-DDLab/ (last modified 21 March 2013).

Choi, W.S., Sandlöbes, S., Malyar, N.V., Kirchlechner, C., Korte-Kerzel, S., Dehm, G., Choi, P.P., Raabe, D., 2018. On the nature of twin boundary-associated strengthening in Fe-Mn-C steel. Scr. Mater. 156, 27-31.

Choi, W.S., Sandlöbes, S., Malyar, N.V., Kirchlechner, C., Korte-Kerzel, S., Dehm, G., De Cooman, B.C., Raabe, D., 2017. Dislocation interaction and twinning-induced plasticity in

face-centered cubic Fe-Mn-C micro-pillars. Acta Mater. 132, 162-173.

Cui, Y.N., Liu, Z.L., Zhuang, Z., 2015. Theoretical and numerical investigations on confined plasticity in micropillars. J. Mech. Phys. Solids. 76, 127-143.

Cui, Y.N., Lin, P., Liu, Z.L., Zhuang, Z., 2014. Theoretical and numerical investigations of single arm dislocation source controlled plastic flow in FCC micropillars. Int. J. Plast. 55, 279-292.

Dancette, S., Delannay, L., Renard, K., Melchior, M.A., Jacques, P. J., 2012. Crystal plasticity modeling of texture development and hardening in TWIP steels. Acta Mater. 60, 2135-2145.

De Cooman, B.C., Estrin, Y., Kim, S.K., 2018. Twinning-induced plasticity (TWIP) steels. Acta Mater. 142, 283-362.

El-Awady, J.A., 2015. Unravelling the physics of size-dependent dislocation-mediated plasticity. Nat. Commun. 6, 5926.

Fan, H., Aubry, S., Arsenlis, A., El-Awady, J.A., 2015. The role of twinning deformation on the hardening response of polycrystalline magnesium from discrete dislocation dynamics simulations. Acta Mater. 92, 126-139.

Fan, H., Aubry, S., Arsenlis, A., El-Awady, J.A., 2016. Grain size effects on dislocation and twinning mediated plasticity in magnesium. Scr. Mater. 112, 50-53.

Fu, X., Wu, X., Yu, Q., 2018. Dislocation plasticity reigns in a traditional twinning-induced plasticity steel by in situ observation. Mater. Today Nano. 3, 48-53.

Gao, J., Jiang, S., Zhang, H., Huang, Y., Guan, D., Xu, Y., Guan, S., Bendersky, L., Davydov, A., Wu, Y., Zhu, H., Wang, Y., Lu, Z., Rainforth, W., 2021. Facile route to bulk ultrafine-grain steels for high strength and ductility. Nature. 590, 262-267.

Guo, X.R., Sun, C.Y., Li, R., Guo, N., Wei, Y.C., Su, Z.X., Yan, S.P., 2017. A dislocation density based model for twinning induced softening of TWIP steel. Comput. Mater. Sci. 139, 8-15.

Gutierrez-Urrutia, I., Raabe, D., 2012. Grain size effect on strain hardening in twinning-induced plasticity steels. Scr. Mater. 66, 992-996.

Huang, M., Huang, S., Liang, S., Zhu, Y., Li, Z., 2020. An efficient 2D discrete dislocation Dynamics-XFEM coupling framework and its application to polycrystal plasticity. Int. J. Plast. 127, 102647.

Idrissi, H., Renard, K., Ryelandt, L., Schryvers, D., Jacques, P. J., 2010. On the mechanism of twin formation in Fe-Mn-C TWIP steels. Acta Mater. 58, 2464-2476.

Jin, Z.H., Gumbsch, P., Albe, K., Ma, E., Lu, K., Gleiter, H., Hahn, H., 2008. Interactions between non-screw lattice dislocations and coherent twin boundaries in face-centered cubic metals. Acta Mater. 56, 1126-1135.

Jin, Z.H., Gumbsch, P., Ma, E., Albe, K., Lu, K., Hahn, H., Gleiter, H., 2006. The interaction mechanism of screw dislocations with coherent twin boundaries in different face-centred cubic metals. Scr. Mater. 54, 1163-1168.

Khan, S.M.A., Zbib, H.M., Hughes, D.A., 2004. Modeling planar dislocation boundaries using multi-scale dislocation dynamics plasticity. Int. J. Plast. 20, 1059-1092.

Lavenstein, S., El-Awady, J.A., 2019. Micro-scale fatigue mechanisms in metals: Insights gained from small-scale experiments and discrete dislocation dynamics simulations. Curr. Opin. Solid State Mater. Sci. 23, 100765.

Li, D., Zbib, H., Sun, X., Khaleel, M., 2014. Predicting plastic flow and irradiation hardening of iron single crystal with mechanism-based continuum dislocation dynamics. Int. J. Plast. 52, 3-17.

Li, Y., Zhu, L., Liu, Y., Wei, Y., Wu, Y., Tang, D., Mi, Z., 2013. On the strain hardening and texture evolution in high manganese steels: Experiments and numerical investigation. J. Mech. Phys. Solids. 61, 2588-2604.

Li, Z., Hou, C., Huang, M., Ouyang, C., 2009. Strengthening mechanism in

micro-polycrystals with penetrable grain boundaries by discrete dislocation dynamics simulation and Hall-Petch effect. Comput. Mater. Sci. 46, 1124-1134.

Liang, Z.Y., De Hosson, J.T.M., Huang, M.X., 2017. Size effect on deformation twinning in face-centred cubic single crystals: Experiments and modelling. Acta Mater. 129, 1-10.

Liang, Z.Y., Li, Y.Z., Huang, M.X., 2016. The respective hardening contributions of dislocations and twins to the flow stress of a twinning-induced plasticity steel. Scr. Mater. 112, 28-31.

Liang, Z.Y., Wang, X., Huang, W., Huang, M.X., 2015. Strain rate sensitivity and evolution of dislocations and twins in a twinning-induced plasticity steel. Acta Mater. 88, 170-179.

Liebig, J.P., Krauß, S., Göken, M., Merle, B., 2018. Influence of stacking fault energy and dislocation character on slip transfer at coherent twin boundaries studied by micropillar compression. Acta Mater. 154, 261-272.

Liu, Z.L., Liu, X.M., Zhuang, Z., You, X.C., 2009. A multi-scale computational model of crystal plasticity at submicron-to-nanometer scales. Int. J. Plast. 25, 1436-1455.

Lu, X., Zhao, J., Wang, Z., Gan, B., Zhao, J., Kang, G., Zhang, X., 2020. Crystal plasticity finite element analysis of gradient nanostructured TWIP steel. Int. J. Plast. 130, 102703.

Luo, Z.C., Huang, M.X., 2018. Revisit the role of deformation twins on the work-hardening behaviour of twinning-induced plasticity steels. Scr. Mater. 142, 28-31.

Mahato, B., Sahu, T., Shee, S. K., Sahu, P., Sawaguchi, T., Kömi, J., Karjalainen, L. P., 2017. Simultaneous twinning nucleation mechanisms in an Fe-Mn-Si-Al twinning induced plasticity steel. Acta Mater. 132, 264-275.

Olarnrithinun, S., Chakravarthy, S. S., Curtin, W.A., 2013. Discrete dislocation modeling of fracture in plastically anisotropic metals. J. Mech. Phys. Solids. 61, 1391-1406.

Mianroodi, J. R., Svendsen, B., 2020. Effect of twin boundary motion and dislocation-twin interaction on mechanical behavior in fcc metals. Materials. 13, 2238.

Shen, Y.F., Wang, Y.D., Liu, X.P., Sun, X., Peng, R. L., Zhang, S.Y., Zuo, L., Liaw, P.K., 2013. Deformation mechanisms of a 20Mn TWIP steel investigated by in situ neutron diffraction and TEM. Acta Mater. 61, 6093-6106.

Srivastava, K., El-Awady, J.A., 2017. Deformation of magnesium during c-axis compression at low temperatures. Acta Mater. 133, 282-292.

Steinmetz, D.R., Jäpel, T., Wietbrock, B., Eisenlohr, P., Gutierrez-Urrutia, I., Saeed-Akbari, A., Hickel, T., Roters, F., Raabe, D., 2013. Revealing the strain-hardening behavior of twinning-induced plasticity steels: Theory, simulations, experiments. Acta Mater. 61, 494-510.

Sun, C.Y., Guo, N., Fu, M.W., Wang, S.W., 2016. Modeling of slip, twinning and transformation induced plastic deformation for TWIP steel based on crystal plasticity. Int. J. Plast. 76, 186-212.

You, Z., Li, X., Gui, L., Lu, Q., Zhu, T., Gao, H., Lu, L., 2013. Plastic anisotropy and associated deformation mechanisms in nanotwinned metals. Acta Mater. 61, 217-227.

Wang, J., Stanford, N., 2017. A critical assessment of work hardening in TWIP steels through micropillar compression. Mater. Sci. Eng., A. 696, 42-51.

Wang, P., Xu, S., Liu, J., Li, X., Wei, Y., Wang, H., Gao, H., Yang, W., 2017. Atomistic simulation for deforming complex alloys with application toward TWIP steel and associated physical insights. J. Mech. Phys. Solids. 98, 290-308.

Wei, D., Zaiser, M., Feng, Z., Kang, G., Fan, H., Zhang, X., 2019. Effects of twin boundary orientation on plasticity of bicrystalline copper micropillars: A discrete dislocation dynamics simulation study. Acta Mater. 176, 289-296.

Wei, Y. J., Li, Y.Q., Zhu, L.C., Liu, Y., Lei, X.Q., Wang, G., Wu, Y.X., Mi, Z.L., Liu, J.B., Wang, H.T., Gao, H.J., 2014. Evading the strength-ductility trade-off dilemma in steel through gradient hierarchical nanotwins. Nat. Commun. 5, 1-8.

Wu, Z. X., Zhang, Y.W., Srolovitz, D.J., 2009. Dislocation-twin interaction mechanisms for ultrahigh strength and ductility in nanotwinned metals. Acta Mater. 57, 4508-4518.

Xu, S., Xiong, L., Chen, Y., McDowell, D.L., 2016. Sequential slip transfer of mixed-character dislocations across Σ3 coherent twin boundary in FCC metals: a concurrent atomistic-continuum study. npj Comp. Mater. 2, 15016.

Zhang, H., Dong, X., Du, D., Wang, Q., 2013. A unified physically based crystal plasticity model for FCC metals over a wide range of temperatures and strain rates. Mater. Sci. Eng., A. 564, 431-441.

Zhang, X., Lu, S., Zhang, B., Tian, X., Kan, Q., Kang, G., 2021. Dislocation-grain boundary interaction-based discrete dislocation dynamics modeling and its application to bicrystals with different misorientations. Acta Mater. 202, 88-98.

Zhu, Y.T., Wu, X.L., Liao, X.Z., Narayan, J., Keckés, L.J., Mathaudhu, S.N., 2011. Dislocation-twin interactions in nanocrystalline fcc metals. Acta Mater. 59, 812-821.

Zheng, Z., Balint, D.S., Dunne, F.P.E., 2016. Discrete dislocation and crystal plasticity analyses of load shedding in polycrystalline titanium alloys. Int. J. Plast. 87, 15-31.

Zhou, P., Liang, Z.Y., Liu, R.D., Huang, M.X., 2016. Evolution of dislocations and twins in a strong and ductile nanotwinned steel. Acta Mater. 111, 96-107.

Zhu, Y., Wang, H., Zhu, X., Xiang, Y., 2014. A continuum model for dislocation dynamics incorporating Frank-Read sources and Hall-Petch relation in two dimensions. Int. J. Plast. 60, 19-39.

Ziegler, H., Wehrli, C., 1987. The derivation of constitutive relations from the free energy and the dissipation function. Adv. Appl. Mech. 25, 183-238.